Article

Cell Metabolism

The Translational Machinery of Human CD4+ T Cells Is Poised for Activation and Controls the Switch from Quiescence to Metabolic Remodeling

Graphical Abstract

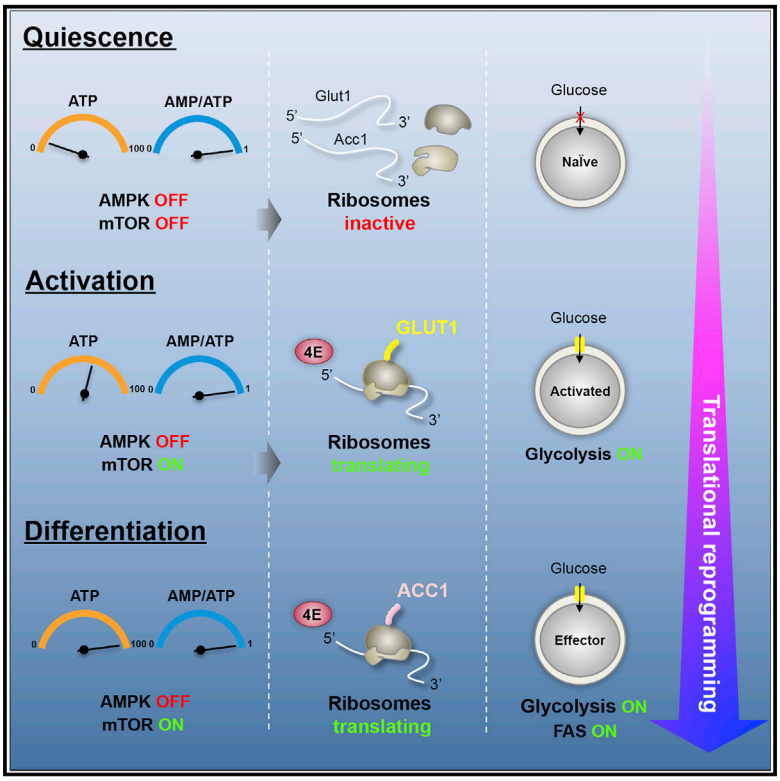

Highlights

- Naive T cells possess a translational machinery poised for immediate protein synthesis
- Quiescent naive T cells accumulate mRNAs for glycolysis and fatty acid synthesis
- Translation regulates GLUT1 and ACC1, bypassing nutrient-sensing repression
- ACC1 translation is necessary for metabolic reprogramming to the effector phenotype

Authors

Sara Ricciardi, Nicola Manfrini, Roberta Alfieri, ..., Massimiliano Pagani, Sergio Abrignani, Stefano Biffo

Correspondence

biffo@ingm.org

In Brief

Ricciardi et al. show that the translation of pre-accumulated mRNAs encoding key players in glycolytic and fatty acid synthesis drives metabolic reprogramming of naive T cells. Upon TCR activation, the poised translational machinery is activated, thereby coordinating the translation of GLUT1 and ACC1 mRNAs and linking metabolism to effector cell fate.

Ricciardi et al., 2018, Cell Metabolism *28*, 895–906
December 4, 2018
https://doi.org/10.1016/j.cmet.2018.08.009

CellPress

Cell Metabolism
Article

The Translational Machinery of Human CD4+ T Cells Is Poised for Activation and Controls the Switch from Quiescence to Metabolic Remodeling

Sara Ricciardi,[1,5,6] Nicola Manfrini,[1,6] Roberta Alfieri,[1] Piera Calamita,[1,5] Maria Cristina Crosti,[1] Simone Gallo,[1] Rolf Müller,[2] Massimiliano Pagani,[1,3] Sergio Abrignani,[1,4] and Stefano Biffo[1,5,7,*]
[1]INGM, National Institute of Molecular Genetics, "Romeo ed Enrica Invernizzi", Via Francesco Sforza 35, Milan 20122, Italy
[2]Helmholtz Institute for Pharmaceutical Research Saarland (HIPS), Helmholtz Center for Infection Research and Department of Pharmacy, Saarland University Campus, Building C2.3, Saarbrücken 66123, Germany
[3]Department of Medical Biotechnology and Translational Medicine, Università degli Studi di Milano, Milan, Italy
[4]Department of Clinical Sciences and Community Health, Università degli Studi di Milano, Milan, Italy
[5]Bioscience Department, Università degli Studi di Milano, Milan, Italy
[6]These authors contributed equally
[7]Lead Contact
*Correspondence: biffo@ingm.org
https://doi.org/10.1016/j.cmet.2018.08.009

SUMMARY

Naive T cells respond to T cell receptor (TCR) activation by leaving quiescence, remodeling metabolism, initiating expansion, and differentiating toward effector T cells. The molecular mechanisms coordinating the naive to effector transition are central to the functioning of the immune system, but remain elusive. Here, we discover that T cells fulfill this transitional process through translational control. Naive cells accumulate untranslated mRNAs encoding for glycolysis and fatty acid synthesis factors and possess a translational machinery poised for immediate protein synthesis. Upon TCR engagement, activation of the translational machinery leads to synthesis of GLUT1 protein to drive glucose entry. Subsequently, translation of ACC1 mRNA completes metabolic reprogramming toward an effector phenotype. Notably, inhibition of the eIF4F complex abrogates lymphocyte metabolic activation and differentiation, suggesting ACC1 to be a key regulatory node. Thus, our results demonstrate that translation is a direct mediator of T cell metabolism and indicate translation factors as targets for novel immunotherapeutic approaches.

INTRODUCTION

In humans, circulating naive T cells are quiescent and their lifespan has been estimated to be years (Michie et al., 1992). Quiescent CD4+ naive T lymphocytes proliferate and differentiate toward effector memory and central memory cell subsets when activated by antigens and cytokines (Geginat et al., 2001). T cell activation and polarization are energetically demanding and require the action of global regulators of translation, growth, and metabolism such as c-Myc (Wang et al., 2011). Consistently, upon T cell receptor (TCR) activation naive CD4+ T cells undergo a metabolic reprogramming simplified into a switch from fatty acid oxidation to glycolysis (Chang et al., 2013; O'Neill et al., 2016; Wang and Green, 2012). Curiously, the observation that quiescent naive cells produce energy through fatty acid oxidation derives from the seminal observation that freshly dissociated rat lymphocytes increase O_2 consumption upon exogenous oleate administration (Ardawi and Newsholme, 1984). These facts raise two questions: (1) how is the metabolic switch to glycolysis rapidly activated starting from a resting state? And (2) in the absence of fatty acid storage capability, how can naive CD4+ T cells deal with an increased input of fatty acids, maintaining quiescence, and avoiding fatty acid synthesis?

Mammalian target of rapamycin (mTOR) is an evolutionarily conserved serine/threonine kinase that acts as a hub to promptly respond to a wide range of environmental cues. mTOR functions in two different complexes, mTORC1 and mTORC2. mTORC1 mainly regulates protein synthesis, metabolism, and protein turnover, and is acutely inhibited by rapamycin; mTORC2, in mammalian cells, controls proliferation, survival, and actin dynamics (Saxton and Sabatini, 2017). mTOR activation follows TCR stimulation and is central for T cell function (Chi, 2012; Powell and Delgoffe, 2010). mTOR activation is essential for T cell commitment to T helper 1 (Th1), Th2, and Th17 effector cell lineages and mTOR-deficient CD4+ T cells preferentially differentiate toward a regulatory (Treg) phenotype (Delgoffe et al., 2009). mTOR inhibitors are immunosuppressants (Budde et al., 2011). Downstream metabolic events induced by mTORC1 activation include glycolysis and fatty acid synthesis (Dibble and Manning, 2013), which are essential for the transition from naive to effector and memory cells (O'Neill et al., 2016). Recently, it was reported that metabolic fluxes of naive CD4+ T cells involve transient fluctuations of L-arginine (Geiger et al., 2016). mTORC1 activity is critically regulated by L-arginine through CASTOR proteins (Chantranupong et al., 2016), suggesting that metabolic reprogramming requires rapid mTORC1 activation through amino acid influx. mTORC1 is regulated by Rheb that is inhibited by tumor suppressors TSC1/2 under the control of the nutrient-sensing kinase AMPK (Howell et al., 2017). When AMPK is stimulated by a high AMP/ATP ratio, it simultaneously inhibits protein and fatty acid synthesis by negatively regulating

mTORC1 and ACC1, respectively (Fullerton et al., 2013). Since quiescent cells may have low energy levels, this generates the paradox that in order to shut off fatty acid synthesis by AMPK, mTORC1 activity would be constitutively inhibited, at odds with the dynamics of T cell activation. Additional mechanisms must therefore exist for regulation of fatty acid synthesis.

mTORC1 contains RAPTOR, whose deletion in mice intriguingly abrogates metabolic reprogramming (Yang et al., 2013). However, one major role of mTORC1 is to regulate initiation of translation (Hsieh et al., 2012; Thoreen et al., 2012). mTORC1 phosphorylates 4E-BPs that, once phosphorylated, dissociate from eIF4E. eIF4E can then be recruited to the eIF4F complex (Sonenberg and Hinnebusch, 2009). The eIF4F complex can drive translation of specific mRNAs (Masvidal et al., 2017). In proliferating cancer cells, the sensitivity of proliferation to rapamycin is abrogated by deletion of 4E-BPs, thus demonstrating the functional impact of mTORC1-mediated 4E-BP phosphorylation (Dowling et al., 2010). eIF4E is also translationally regulated in T cell subsets (Piccirillo et al., 2014). mTORC1 activity can also control other steps of translation, such as elongation (Faller et al., 2015; Wang et al., 2000). Finally, other translation factors such as eIF6 are robustly activated during T cell stimulation (Biffo et al., 1997; Manfrini et al., 2017) and can control growth (Gandin et al., 2008) and metabolic fluxes (Biffo et al., 2018; Brina et al., 2015). These observations suggest that the transition of naive to an activated state is robustly controlled at the translational level. Whether translational control can affect metabolism in T cells is, however, totally unknown.

Here, we developed an unbiased approach based on the combination of transcriptomics, proteomics, and mass spectrometry (MS) analysis of metabolites. Using this strategy we reveal that resting $CD4^+$ naive T cells have a poised ribosomal machinery and an unexpected pre-accumulation of mRNAs encoding for enzymes involved in glycolysis and fatty acid synthesis. Driven by these findings, we re-examined metabolic pathways and conclude that the best model that describes the transition from quiescence to activation is a metabolic awakening that simultaneously induces oxidative phosphorylation, glycolysis, and fatty acid synthesis due to sequential translational activation of the glucose transporter GLUT1 and the acetyl-coenzyme A (CoA) carboxylase ACC1. Intriguingly, despite robust changes in ATP concentration, human $CD4^+$ naive T cells keep the AMP/ATP ratio constant, and regulate ACC1 activity relying on translational repression rather than AMPK-mediated phosphorylation.

RESULTS

Transcriptomics of Human $CD4^+$ T Cells Are at Odds with Their Metabolic Features, and Fatty Acid Synthesis Is Controlled by Post-transcriptional Shut-Off of ACC1

Differences in metabolism are key features of human $CD4^+$ and $CD8^+$ T subsets (O'Neill et al., 2016; Vazquez et al., 2016). We collected mRNA expression data of human primary lymphocyte subtypes. We used a dataset of 63 RNA sequencing (RNA-seq) samples from 13 resting human lymphocyte subsets (Bonnal et al., 2015) to unveil the mechanistic networks that control metabolic switches. We classified metabolic enzymes taking into account rate-limiting steps (Table S1), and interrogated the human lymphocyte dataset for mRNA expression of metabolic genes (Table S2). Pearson correlation of metabolic pathways across T cell subsets confirmed metabolic signature similarities within effector naive $CD4^+$ and $CD8^+$ T cells, demonstrating that the new clustering of metabolic pathways identifies consistent populations (Figure 1A).

Strikingly, a close inspection of the metabolic pathways of resting $CD4^+$ naive T cells revealed features of mRNA abundance that are at odds with naive $CD4^+$ resting metabolism. In short, $CD4^+$ naive T cells show high levels of mRNAs encoding for glycolysis (Figure 1B), fatty acid synthesis (Figure 1C), and *de novo* purine synthesis (Figure S1A) enzymes. Next, we challenged the obvious hypothesis that metabolism is post-transcriptionally regulated in $CD4^+$ T cells. To do so, we first performed a meta-analysis of transcriptomic and proteomic datasets (Mitchell et al., 2015) of metabolic genes in $CD4^+$ naive T cells (Table S2), followed by validation strategies. The analysis revealed that the protein/mRNA ratio of each metabolic factor varied conspicuously. Genes with a $1.00 \times 10^{-8} \leq$ iBAQ were considered absent at the protein level. Fifteen genes met these criteria (Figure 1D). Among them, we found the glucose transporter GLUT1, which mediates glucose entry in T cells after activation (Macintyre et al., 2014), and acetyl-CoA carboxylase ACC1, which catalyzes the carboxylation of acetyl-CoA to malonyl-CoA, the rate-limiting step in fatty acid synthesis (Figures 1E and 1F). Thus, the high glycolytic and fatty acid synthesis capabilities, as detected by mRNA levels in $CD4^+$ naive T cells, are not matched by protein expression. We then asked whether post-transcriptional silencing of metabolic rate-limiting enzymes is a consistent feature of T cell subsets. Strikingly, both GLUT1 and ACC1 were expressed at comparable mRNA levels in all $CD4^+$ T cell subsets (Figures S1B and S1C). By contrast, GLUT1 and ACC1 proteins were undetectable in resting $CD4^+$ naive T cells but detectable in other $CD4^+$ T cell subsets as indicated by fluorescence-activated cell sorting (FACS) analysis for GLUT1 (Figure 1G) and western blot for ACC1 (Figure 1H). These data unequivocally demonstrate that post-transcriptional control is a major layer of regulation in the metabolism of T cell subsets, raising the question of whether the control is at the translational level.

Human $CD4^+$ T Cells Have a High Ribosomal Capability that Is Poised at the Level of Pre-initiation of Translation

The most abundant products of the protein-synthesis apparatus are ribosomes (Rudra and Warner, 2004). First, we reannotated and categorized the proteins involved in ribosomal production (Henras et al., 2008) into four groups: RNA polymerases, proteins of the small ribosomal subunit (RPSs), proteins of the large ribosomal subunit, and ribosome *trans*-acting factors (Table S3). Based on their abundance at the mRNA level, we introduced the Ribosome Capability Index. We observed high ribosomal capability in $CD4^+$ naive T cells and $CD4^+$ central memory T cells and low ribosomal capability in all $CD4^+$ glycolytic effector T cells (Figure 2A; Table S4). We further performed a meta-analysis of transcriptomic and proteomic data of $CD4^+$ naive T cells (Mitchell et al., 2015) (Table S4). The analysis revealed concordance between the mRNA and protein levels of ribosomal and *trans*-acting factor genes (Figures 2B, 2C, S2A, and S2B), demonstrating the unexpected abundance of the ribosomal machinery in $CD4^+$ naive T cells compared with effector subsets.

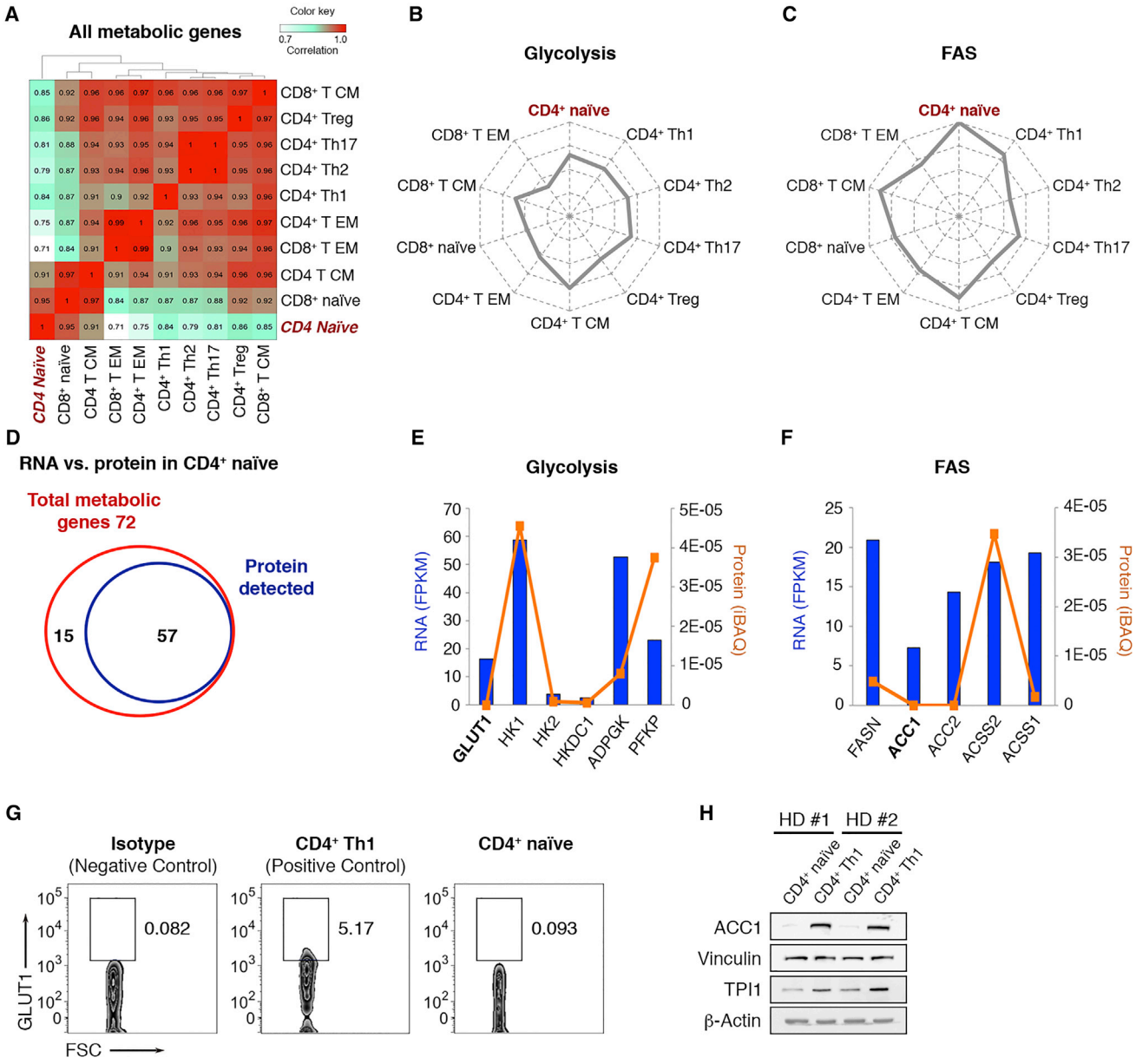

Figure 1. CD4⁺ Naive T Cells Present High Glycolytic and Fatty Acid Synthesis Potentials at the Steady-State mRNA Level but Remain Quiescent by Regulating the Expression of Key Glycolytic and Fatty Acid Synthesis Enzymes

(A) Heatmap showing the pairwise Pearson correlation coefficient of the $\log_2$ read count of all metabolic genes across CD4⁺ and CD8⁺ T cell subsets (Pearson correlation coefficient 0.7–1 between cell subsets).

(B and C) Radar charts of the distribution of gene expression calculated for glycolysis (B) and fatty acid synthesis (FAS) (C). In the radar charts T cell subsets are represented by axes originating from the same point and metabolic pathways are represented by a spoke. The length of a spoke is proportional to the magnitude of the metabolic pathway. Naive cells have the highest levels of mRNAs encoding for FAS among all T subsets.

(D) Venn diagram showing the number of metabolic genes expressed at the protein level. Fifteen genes were absent at the protein level.

(E and F) Correlation bar plots of iBAQ intensities (proteome) versus FPKM values (transcriptome) of glycolysis (E) and FAS genes (F). Naive cells have high mRNA levels of GLUT1 and ACC1, but no proteins.

(G) Flow cytometry plots representative of three experiments showing the expression of GLUT1 protein in CD4⁺ naive and CD4⁺ Th1 cells isolated from peripheral blood.

(H) The immunoblot of ACC1 protein in CD4⁺ naive and CD4⁺ Th1 cells isolated from peripheral blood of two healthy donors shows absence of ACC1 protein in naive compared with Th1 cells.

Next, we analyzed the translation machinery. We reannotated and categorized the proteins involved in translation (Henras et al., 2008) into ten clusters, i.e., start codon accuracy, eIF2 exchange, ternary complex, RNA assistance by eIF3, cap translation inhibition, cap binding, helicase activity, ribosome subunit joining, elongation, and termination (Table S5), and interrogated

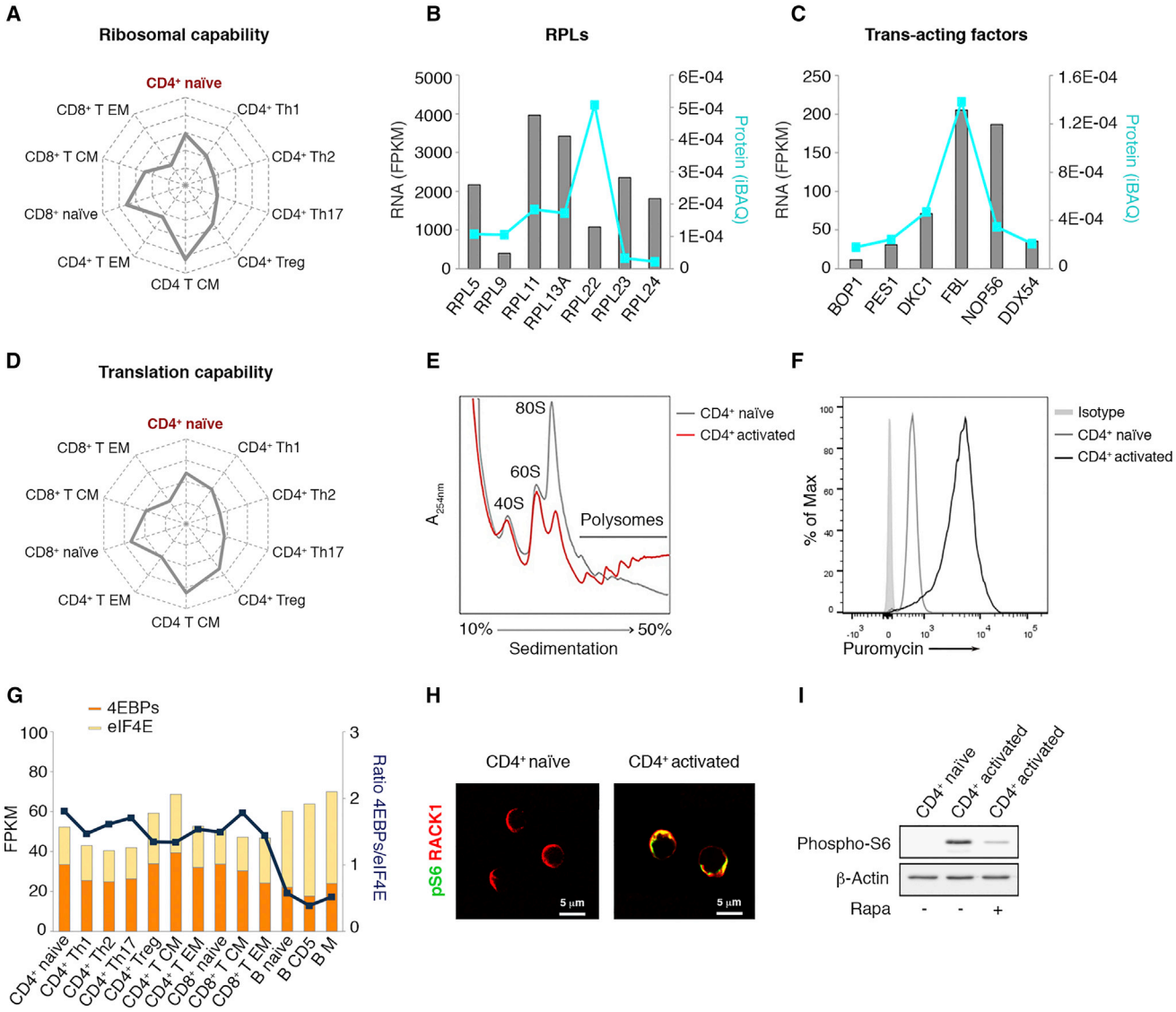

Figure 2. CD4⁺ Naive T Cells Have a Conspicuous but Poised Ribosomal Machinery that Is Activated by T Cell Receptor Stimulation

(A) Radar chart of the distribution of ribosomal genes across CD4⁺ and CD8⁺ T cell subsets. T cell subsets are represented by axes originating from the same point and ribosomal capability is represented by a spoke. The length of a spoke is proportional to the magnitude of the ribosomal capability. Naive and central memory cells have the highest levels of ribosomal mRNAs.

(B and C) Correlation bar plots of iBAQ intensities (proteome) versus FPKM values (transcriptome) of L ribosomal proteins (RPLs) (B), and *trans*-acting factor (C) genes. All ribosome-associated genes are abundant at the protein level.

(D) Radar chart of the distribution of translational control genes across CD4⁺ and CD8⁺ T cell subsets. T cell subsets are represented by axes originating from the same point and translation capability is represented by a spoke. The length of a spoke is proportional to the magnitude of the translation capability.

(E) Polysomal profiles of CD4⁺ naive or activated CD4⁺ T cells. A high 80S peak is a marker of inactive translation. Upon TCR stimulation, 80S subunits are converted in active polysomes and the 80S peak drops.

(F) Flow cytometry histogram representative of three experiments showing puromycin incorporation in CD4⁺ naive and CD4⁺ T cells activated for 72 hr. Protein synthesis increases upon consistent TCR stimulation.

(G) Bar graph showing the values of the 4EBPs/eIF4E ratios in T and B lymphocyte subsets predicts the translational sensitivity to rapamycin of all T cell subsets, but not of B cells.

(H) The ribosomal machinery is activated by TCR stimulation. Representative immunofluorescence of three experiments of phospho-rpS6 (green) and RACK1 (red) proteins in CD4⁺ naive or activated CD4⁺ T cells. RACK1 is a structural marker of the 40S subunit, and phospho-rpS6 is the phosphorylated form of the 40S ribosomal protein S6, a marker of mTORC1-S6K cascade. Scale bars, 5 μm.

(I) Representative immunoblot of two independent experiments of the phospho-rpS6 protein in CD4⁺ T cells activated in the presence of rapamycin. Rapamycin blocks mTORC1-dependent rpS6 phosphorylation.

the RNA-seq dataset for mRNA expression levels of the translation genes described above (Table S5). Analysis of $CD4^+$ naive T cells revealed high levels of elongation factors but low levels of rate-limiting initiation factors such as eIF4E and eIF6 (Figure S2C), with $CD4^+$ naive T cells presenting a consistent translational apparatus when compared with effector subsets (Figure 2D). In conclusion, our data rule out that the paucity of ribosomes explains undetectable ACC1 or GLUT1, but rather suggest that naive T cells have a conspicuous ribosomal capability.

We analyzed the activity status of ribosomes of naive cells. Polysomal profiles of $CD4^+$ naive cells showed a high 80S peak, a hallmark of absence of translation initiation. TCR stimulation led to a rapid decrease of the 80S peak with a concomitant rise of polysomes (Figure 2E), an indication of active translation initiation. Quantification of protein synthesis by flow-sorting enriched puromycin $CD4^+$ naive and $CD4^+$ T cells activated for 72 hr confirmed that the translation machinery is activated upon TCR stimulation (Figure 2F).

Further analysis of translation genes revealed that all T lymphocyte subsets have a high 4E-BPs/eIF4E protein ratio (Figure 2G). At the protein level, 4E-BPs outnumber eIF4E (Figure S2D). Given that phosphorylation of 4E-BPs by mTORC1 results in its dissociation from eIF4E, promoting assembly of the eIF4F complex, these results suggest that, in the absence of mTORC1 activation, T lymphocytes are impaired in eIF4E-dependent translation initiation. A poised translational machinery was further demonstrated by immunofluorescence. We readily detected proxy 40S structural ribosomal protein RACK1 (Ceci et al., 2003) in the cytoplasm of $CD4^+$ naive T cells (Figure 2H), but not phosphorylation of ribosomal protein rpS6, a proxy for mTORC1 activation. TCR stimulation led to phosphorylation of rpS6 and co-localization of phosphorylated rpS6 with RACK1 (Figure 2H). Rapamycin inhibition almost totally prevented phosphorylation of rpS6 (Figure 2I). In conclusion, $CD4^+$ naive T cells have a conspicuous but poised ribosomal machinery that is activated by TCR stimulation.

Translation Activation of GLUT1 and ACC1 Is an Essential Step for Metabolic Reprogramming

We analyzed RNA and protein levels of GLUT1 and ACC1 in $CD4^+$ T cells stimulated *in vitro* (Figure 3A). We found a progressive accumulation of GLUT1-positive cells peaking at 48 hr (Figure 3A) and a progressive accumulation of the ACC1 protein (Figure 3B). By contrast, mRNA levels of both GLUT1 and ACC1 (Figure 3C) sharply increased at 24 hr and then declined, suggesting that each gene had a differential post-transcriptional regulation. We evaluated the impact of translation in the accumulation of GLUT1 and ACC1 protein levels by analyzing the distribution of GLUT1 and ACC1 mRNAs on polysomal gradient fractions of $CD4^+$ naive and $CD4^+$ T cells stimulated at different time points (Figure 3D, left). The analysis showed that the majority of GLUT1 and ACC1 mRNAs are present on subpolysomes in $CD4^+$ naive T cells (Figure 3D, right). By contrast, TCR stimulation promotes the recruitment of GLUT1 and ACC1 mRNAs to active translating polysomes (Figure 3D). To definitively prove that *de novo* protein synthesis is required for GLUT1 and ACC1 protein accumulation upon TCR stimulation, we stimulated $CD4^+$ naive T cells *in vitro* in the presence of either actinomycin D, which blocks transcription, or cycloheximide, which blocks translation (Figures 3E and 3F). Notably, for both GLUT1 (Figure 3E) and ACC1 (Figure 3F) the impact of cycloheximide on protein expression was more pronounced than that of actinomycin D. Together, these results show that key regulators of glycolysis and fatty acid synthesis are mostly regulated at the level of translational accumulation. This finding bears two consequences: (1) quiescence is controlled by repression of translation; (2) the unique repertoire of enzymes present in the cytoplasm of $CD4^+$ naive T cells suggests that the internal metabolic milieu of resting naive cells may be driven by the specific expression of selected metabolic enzymes.

Metabolomic Analysis Demonstrates that in Human Quiescent $CD4^+$ T Cells ACC1 Translational Control Bypasses the Need for AMPK-Driven Pathways

In light of the current view depicting $CD4^+$ naive T cells as quiescent cells relying on fatty acid oxidation (Ardawi and Newsholme, 1984), the high ribosomal, glycolytic, and fatty acid synthesis (FAS) potentials at the steady-state mRNA level of resting $CD4^+$ naive cells were particularly surprising. In addition, FAS has long been known to be associated with cell-cycle progression and growth (Rohrig and Schulze, 2016). Therefore, we hypothesized that in $CD4^+$ naive T cells a sophisticated translational program represses specific metabolic processes. We therefore quantitated by a comprehensive metabolomics study the steady-state levels of inner metabolites both *ex vivo* and during T cell activation (Figure 4A; Table S6). In brief, we found that naive T cells have a peculiar metabolic profile, which is consistent with translational repression of several factors and that, as expected, TCR stimulation led to a complex metabolic reprogramming within 72 hr (Figures 4A and S3A). Among others, quiescent naive cells had (1) high levels of aspartate with no urea, suggesting aspartate use in other pathways (Cardaci et al., 2015), and in general, accumulation of specific amino acids such as glutamine and its metabolites (Figure S3B); (2) low intracellular levels of leucine (Wolfson et al., 2016), consistent with mTORC1 inactive complex (Figure S3C); (3) low levels of lactic acid, citric acid, and ATP (Figure S3D), consistent with quiescence; (4) low levels of glucose metabolism intermediates, such as fructose 1,6-bisphosphate (Figure 4B), consistent with GLUT1 silencing; and (5) absence of malonyl-CoA (Figure 4C), the product of ACC1-catalyzed reaction. After TCR activation, both expected and unexpected events were observed. In brief, (1) intermediates of the Krebs cycle, such as citric acid, and the oxygen consumption rate (OCR) increased in parallel with lactic acid and ATP levels, demonstrating that both respiration and glycolysis are triggered (Figures 4D, 4E, and S3D); (2) there was an increase, at 24 hr, of fructose 1,6-bisphosphate, a conversion product of glucose influx that correlates with GLUT1 accumulation (Figure 4B); (3) subsequent appearance, at 72 hr, of malonyl-CoA, the end product of the reaction catalyzed by ACC1 (Figure 4C) that correlates with ACC1 accumulation (Figure 3B); and most strikingly, (4) the adenylate energy charge never changed despite a 10-fold increase in ATP (Figures 4F and S3D). This last result is relevant in the context of ACC1 translational repression. In $CD4^+$ T cells, since the AMP/ATP ratio remains almost constant the ACC1 catalytic activity is not inhibited by AMPK phosphorylation, as observed in other organs

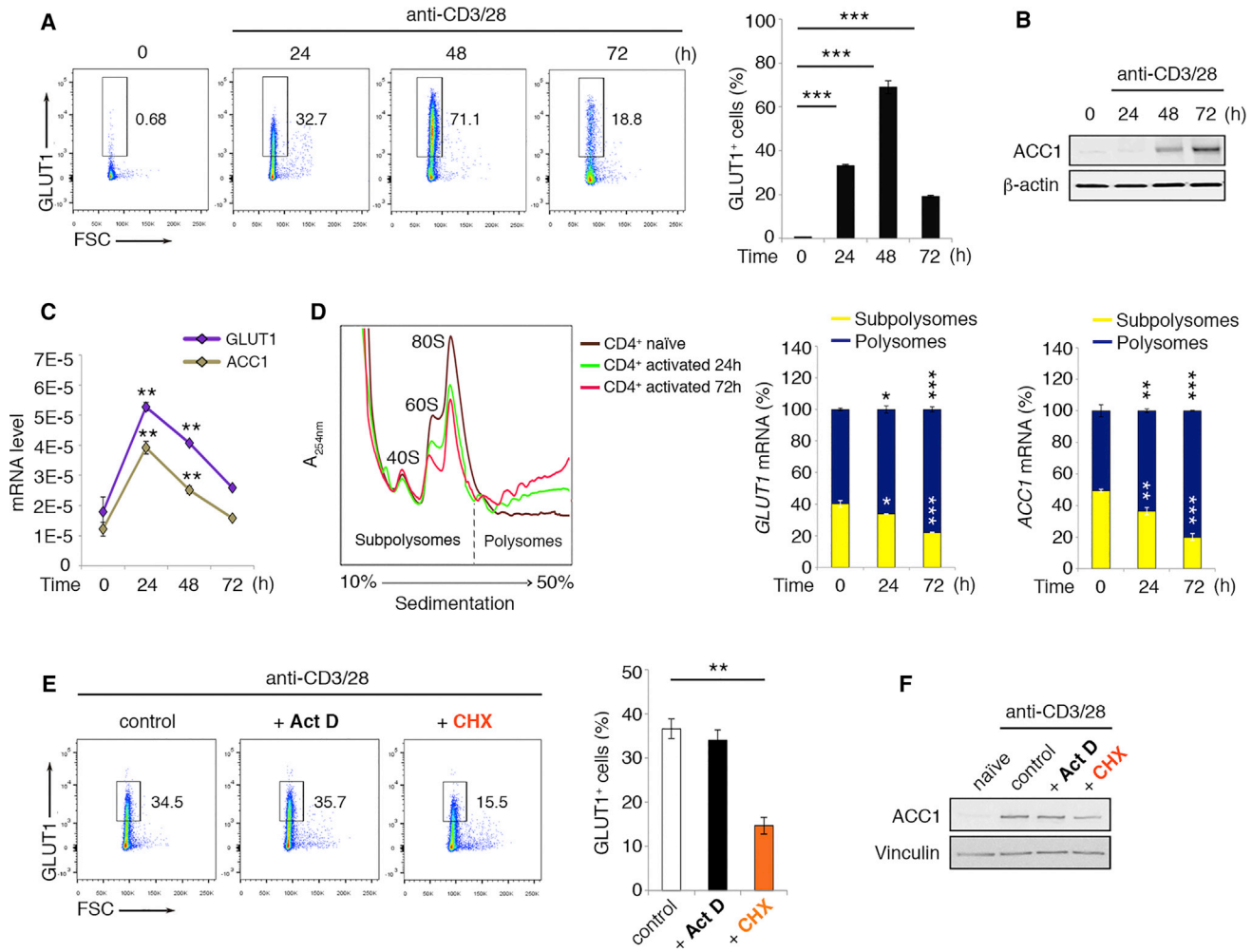

Figure 3. GLUT1 and ACC1 Expression Is Translationally Controlled during Activation of CD4$^+$ T Cells *In Vitro*

(A) Flow cytometry plots representative of three independent experiments showing the expression of GLUT1 protein in CD4$^+$ naive T cells or in the same cells activated for 24, 48, and 72 hr. Right: quantification of flow cytometry data. Data are presented as means ± SD; p values are determined by two-tailed Student's t test. ***p < 0.001.

(B) Immunoblot representative of four independent experiments showing ACC1 protein expression in CD4$^+$ T cells following activation at the indicated time points.

(C) Expression levels of GLUT1 and ACC1 mRNAs in CD4$^+$ naive T cells and in the same cells activated for 24, 48, and 72 hr. Data are presented as means ± SD; p values are determined by two-tailed Student's t test. **p < 0.01.

(D) Polysomal profiles of CD4$^+$ naive and CD4$^+$ T cells stimulated *in vitro* for 24 and 72 hr. Right: quantification of mRNA levels of triplicates in subpolysomes and polysomes showing an increase in polysome-associated GLUT1 and ACC1 transcripts in response to TCR stimulation (CD4$^+$ T cells for each replicate were obtained from three healthy donors). Data are presented as means ± SD; p values are determined by two-tailed Student's t test (CD4$^+$ stimulated versus CD4$^+$ naive T cells). *p < 0.05, **p < 0.01, ***p < 0.001.

(E) Flow cytometry plots representative of three experiments showing the expression of GLUT1 in CD4$^+$ T cells activated in the presence of either actinomycin D (Act D) or cycloheximide (CHX). Right: quantification of flow cytometry data. Data are presented as means ± SD; p values are determined by two-tailed Student's t test. **p < 0.01. Data show that transcriptional inhibition by Act D does not reduce the number of GLUT1$^+$ cells, whereas translational inhibition by CHX does.

(F) Immunoblot representative of two independent experiments showing ACC1 expression in CD4$^+$ T cells activated in the presence of either Act D or CHX. Transcriptional inhibition by Act D does not reduce ACC1 levels, whereas translational inhibition by CHX does.

(Fullerton et al., 2013) (Figure S4A). We conclude that in CD4$^+$ T cells translational repression of ACC1 bypasses AMPK-driven control, avoiding a negative feedback of AMPK on mTORC1 activation. Overall, our data demonstrate that the metabolome of quiescent naive T cells is dictated by the post-transcriptional regulation of metabolic enzymes, raising the question of what the mechanism, and its relevance, may be.

ACC1 Translation Is under the Control of eIF4E Initiation Factor and the Production of Its End Product Malonyl-CoA Is Essential for Full Metabolic Reprogramming of T Cells

Our data indicate that the metabolic quiescence of resting CD4$^+$ naive T cells is regulated by the shut-off of key enzymes and that the transition from metabolic quiescence to activation relies on

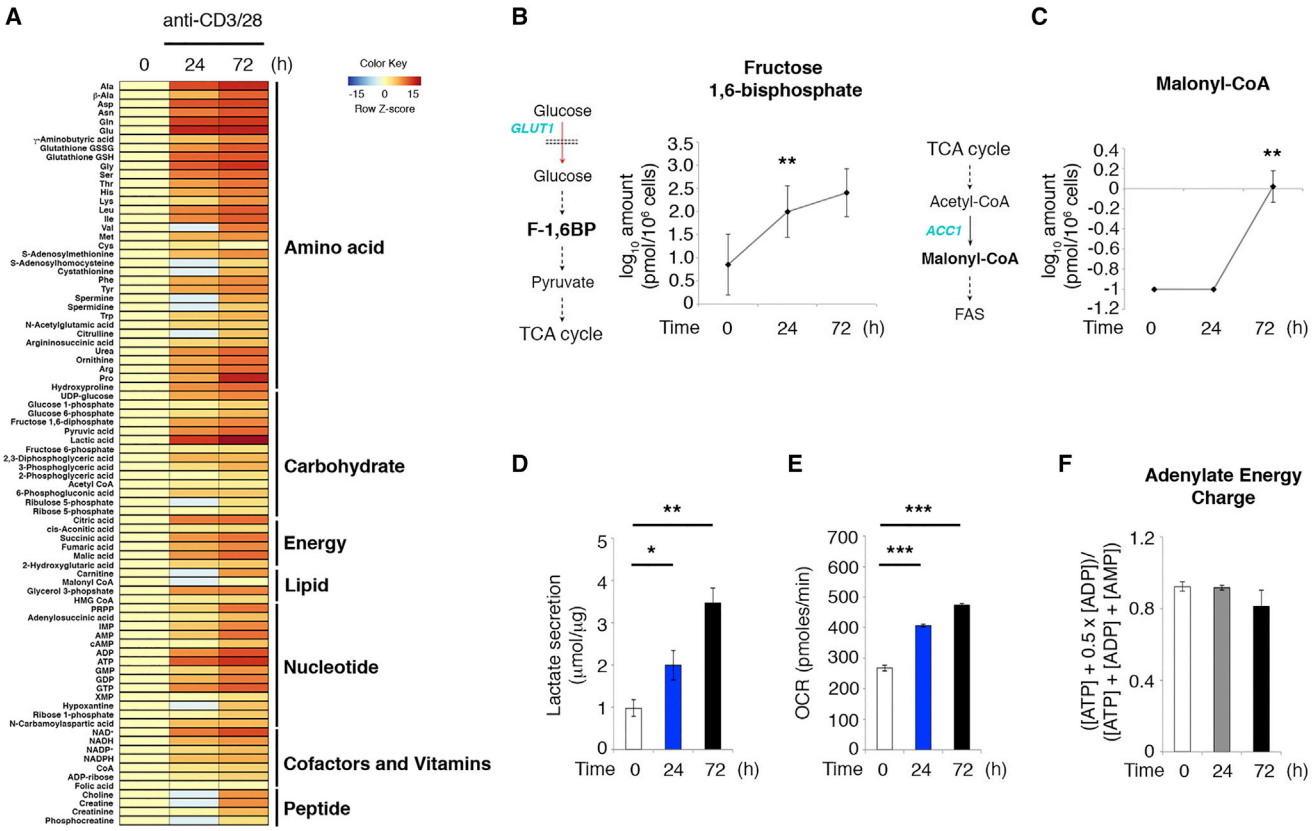

Figure 4. Human CD4$^+$ T Cells Undergo Metabolic Reprogramming through Sequential Activation of Glycolysis, Oxygen Consumption, and FAS without Changes in AMP/ATP Ratios

(A) Metabolome analysis of CD4$^+$ T cells collected at the indicated time points after TCR stimulation. The $\log_2$ value for each metabolite represents the average of triplicates. Metabolites were clustered in seven categories. Clusters are shown.

(B and C) Intracellular concentrations of fructose 1,6-bisphosphate (B) and malonyl-CoA (C) in activated CD4$^+$ T cells. Data represent the average of three replicates (CD4$^+$ T cells for each replicate were derived from five healthy donors). Data are presented as means ± SD; p values are determined by two-tailed Student's t test. **p < 0.01. Accumulation of the two products correlates with translational expression of GLUT1 and ACC1.

(D) Lactate secretion of activated CD4$^+$ T cells. Data represent the average of triplicates (CD4$^+$ T cells for each replicate were obtained from two healthy donors). Data are presented as means ± SD; p values are determined by two-tailed Student's t test. *p < 0.05, **p < 0.01.

(E) OCR of activated CD4$^+$ T cells. Data represent the average of triplicates (CD4$^+$ T cells for each replicate were obtained from two healthy donors). Data are presented as means ± SD; p values are determined by two-tailed Student's t test. ***p < 0.001.

(F) Adenylate energy charge in activated CD4$^+$ T cells. Data represent the average of triplicates.

the translational derepression of key glycolytic and FAS factors. Therefore, the switch from fatty acid oxidation to glycolysis should be considered in the more general context of metabolic awakening of a quiescent cell due to translational activation of pre-existing mRNAs. TCR activation causes rapid mTORC1 activation. Given that mTORC1 controls the formation of the eIF4F complex (Sonenberg and Hinnebusch, 2009), we wondered whether GLUT1 and ACC1 translation might be regulated by the assembly of the eIF4F complex. We employed 4EGi-1, an inhibitor of eIF4E-eIF4G interaction (Figure 5A) (Moerke et al., 2007). 4EGi-1 induced a decrease in the polysomal occupancy of both ACC1 and GLUT1 transcripts (Figures 5B and S5A) and completely prevented the accumulation of ACC1 at the protein level (Figure 5C). As a control, no significant reduction of the expression of RACK1 or eIF6 was detected following 4EGi-1 administration (Figure S5B). Moreover, acute mTORC1 inhibition by rapamycin inhibited GLUT1 and ACC1 in a similar fashion as 4EGi-1 (Figures S5C–S5E). Accordingly, the expression of ACC1 is markedly inhibited also when silencing directly eIF4E (Figure S5F).

The translation of mRNAs bearing long and highly structured 5′ UTRs is strongly dependent on eIF4F. The 5′ UTR of ACC1 is highly structured (Figure 5D) and conserved among several species, suggesting a regulatory role for this region. Indeed, elements that regulate translation have already been identified within the ACC1 5′ UTR. To further investigate the molecular mechanism of ACC1 translational control, we performed a luciferase assay in cultured human cells. The 5′ UTR of ACC1 isoform 2, lacking the internal ribosome entry site structure, was cloned upstream of the *Renilla* luciferase coding sequence in a plasmid expression vector (pRL) and transfected in HEK293 cells. Following a 24-hr growth period, cells were treated with 4EGi-1 and harvested for luciferase assays. As shown in Figure 5E, upon 4EGi-1 treatment the 5′ UTR sequence of ACC1 caused a marked decreased in *Renilla* luciferase activity, as

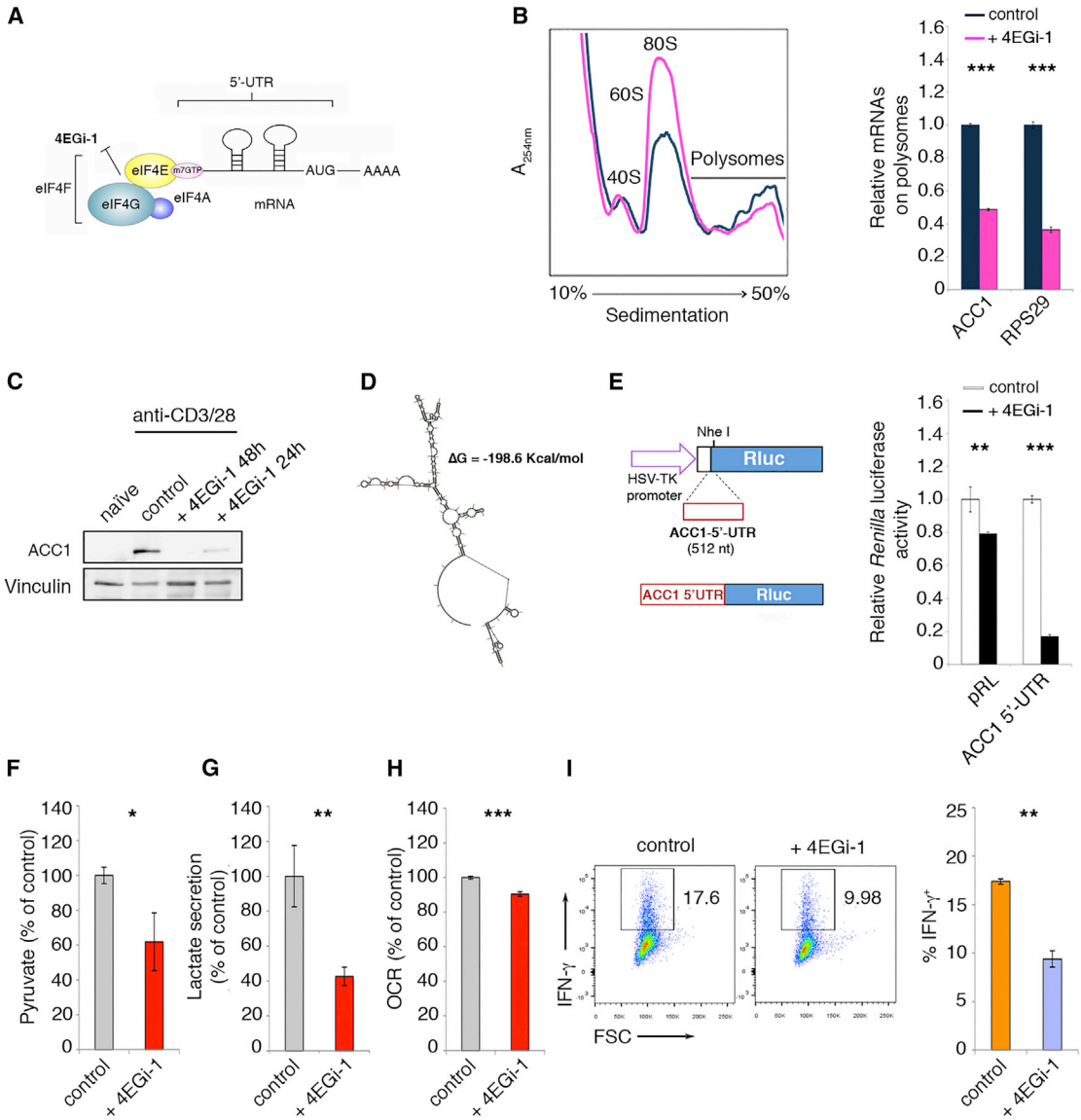

Figure 5. Translational Activation of ACC1 via eIF4E Sustains a Metabolic Feedforward Loop that Completes the Metabolic Reprogramming to an Effector Phenotype

(A) Schematic drawing illustrating the inhibitory effect of 4EGi-1 on translation initiation. 4EGI-1 binds to eIF4E and inhibits eIF4E-eIF4G interaction.

(B) Polysomal profiles of CD4$^+$ T cells activated in the absence or presence of 4EGi-1. Right: quantification of polysome bound ACC1 and RPS29 mRNA levels of three replicates (CD4$^+$ T cells for each replicate were obtained from two healthy donors). Data are presented as means ± SD; p values are determined by two-tailed Student's t test. ***p < 0.001.

(C) Immunoblot representative of three experiments showing ACC1 expression in CD4$^+$ T cells activated in the presence of 4EGi-1. ACC1 expression depends on eIF4F activation.

(D) Predicted secondary structure of the 5′ UTR sequence of ACC1 mRNA.

(E) Schematic of the reporter designed to assess the effect of ACC1 5′ UTR on *Renilla* luciferase protein expression. Right: quantification of three replicates of the relative *Renilla* luciferase activity of pRL and ACC1 5′ UTR constructs in the absence (control) or presence of 4EGi-1. Data are presented as means ± SD; p values are determined by two-tailed Student's t test. **p < 0.01, ***p < 0.001.

(F–H) 4EGi-1 treatment reduces the glycolytic intermediates pyruvate (F) and lactate (G), and respiration (H). Data represent the average of three replicates. Data are presented as means ± SD; p values are determined by two-tailed Student's t test. *p < 0.05, **p < 0.01, ***p < 0.001.

(I) Flow cytometry plots representative of three independent experiments showing IFN-γ production in CD4$^+$ T cells activated in the absence or presence of 4EGi-1. Right: quantification of flow cytometry data. Data are presented as means ± SD; p values are determined by two-tailed Student's t test. **p < 0.01.

compared with a control lacking the 5′ UTR. Thus, the 5′ UTR of ACC1, in its native context, confers the sensitivity of ACC1-RNA translation to eIF4E/eIF4G binding.

Next, we assessed the general impact of eIF4F inhibition on metabolic remodeling of T cells. Intriguingly, administration of 4EGi-1 reduced pyruvate (Figure 5F), lactate (Figure 5G), and

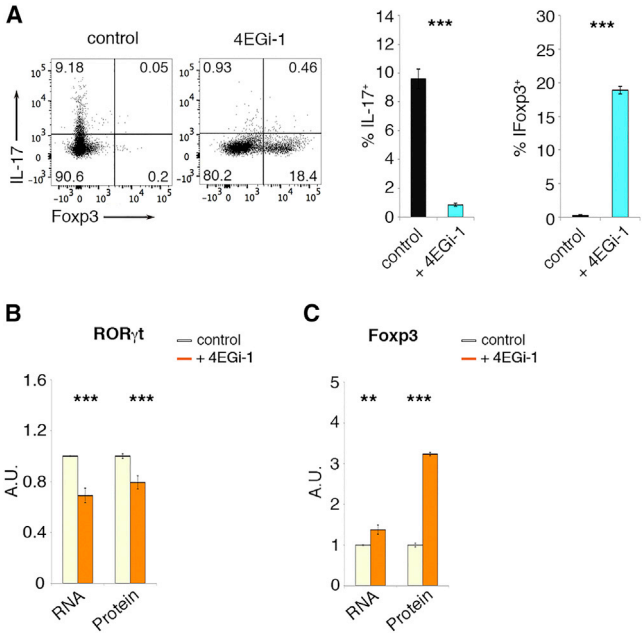

Figure 6. eIF4E-Dependent ACC1 Translation Inhibition Constrains Th17 Cell Polarization toward Anti-inflammatory Foxp3$^+$ Regulatory T Cells

(A) Flow cytometry plots representative of three independent experiments showing IL-17 and Foxp3 in Th17 differentiating cells in the absence or presence of 4EGi-1. Right: quantification of flow cytometry data. Data are presented as means ± SD; p values are determined by two-tailed Student's t tests. * * *p < 0.001.

(B and C) Translation of RORγt and Foxp3 is independent of eIF4F complex formation in Th17 differentiating cells. Bar graphs of three replicates showing relative mRNA (qRT-PCR) and protein levels (FACS) of either RORγt (B) or Foxp3 (C) in Th17 differentiating cells in the absence or presence of 4EGi-1. Data are presented as means ± SD; p values are determined by two-tailed Student's t test. **p < 0.01, ***p < 0.001.

the OCR of activated T cells (Figure 5H), suggesting either a crosstalk of malonyl-CoA synthesis, and therefore of FAS, with glycolysis and respiration, or a broader effect in blocking translation.

We discriminated between the two hypotheses by culturing CD4$^+$ T cells *in vitro* in the presence of soraphen A (SorA) (Jump et al., 2011), a specific inhibitor of the ACC1 isozyme, and analyzed the influence of SorA in the activation-driven changes of cellular metabolism. Pharmacological inhibition of ACC1 was confirmed by the absence of malonyl-CoA in SorA-treated cells. We found that inhibition of ACC1 reduced the activation-driven changes of cellular metabolism and induced a lowering of pyruvate, lactate secretion, and the OCR (Figures S5G–S5I). Thus, malonyl-CoA generation is an important node that crosstalks with the glycolytic pathway. We conclude that the translational control of ACC1 is essential for a full metabolic reprogramming that crosstalks with both respiration and glycolysis.

Our metabolomics and translation data indicate that transition from a resting to an activated state does not operate with a metabolic switch favoring only glycolysis but rather metabolism *in toto* with the tight regulation of ACC1. We then asked what the effects were of 4EGi-1 administration on the capability of naive cells to acquire effector functions at the end of the metabolic reprogramming window. 4EGi-1 administration was accompanied by a significant reduction in the percentage of interferon-γ (IFN-γ)-producing CD4$^+$ T cells (Figure 5I). When we analyzed proliferation, we found only a slight deficit in 4EGi-1-treated cells compared with untreated cells (Figure S5J), indicating that the inhibitory effect on CD4$^+$ T cells differentiation is not a mere consequence of reduced proliferation.

Translational Control May Act at Various Stages of T Cell Differentiation

The surprising observation that metabolic fluxes are ready to be activated by translationally driven mechanisms, coupled with the observation that equal amounts of mRNAs of ACC1 in Th subsets do not reflect equal amounts of proteins, prompt us to ask whether translational control may act also in other developmental decisions. We challenged this hypothesis by studying Th17 and Treg subsets. In brief, we pulsed cells in conditions of polarization to Th17 with 4EGi-1, and verified the expression of interleukin-17 (IL-17) and of Foxp3 (Figure 6A). We found that 4EGi-1 administration reduces the number of T cells expressing IL-17 and increases the amount of cells expressing Foxp3. We analyzed also the expression of IL-17 and Foxp3 after impairing eIF4F complex formation by silencing the expression of eIF4E (Figure S6A). As found in the case of 4EGi-1 administration, also silencing of eIF4E restrains differentiation of Th17 cells and promotes the development of cells expressing Foxp3 (Figure S6A). This result proves the relevance of translational control in CD4$^+$ T cell fate decision.

Finally, we ascertained whether 4EGi-1 might affect the expression of transcription factors crucial for Th17 and Treg cell differentiation. To this end, we analyzed the expression at both protein and mRNA levels of RORγt, which controls Th17 cell differentiation and Foxp3, a well-known transcription factor involved in Treg differentiation, upon 4EGi-1 administration. RORγt decreased both at the mRNA (RORc) and protein level (RORγt) (Figure 6B). Likewise, the increase of Foxp3 at the protein level parallels its increase at the mRNA level (Figure 6C), clearly demonstrating that the expression of both RORγt and Foxp3 is independent of eIF4F complex formation.

DISCUSSION

In brief, we show that human resting CD4$^+$ naive T cells have, at the steady-state mRNA level, an unexpected potential for glycolysis and FAS. Surprisingly, these metabolic pathways are shut off at the translational level. A robust but poised translational machinery is responsible for the sequential activation of metabolic pathways necessary for T cell activation and polarization. Furthermore, inhibition of eIF4F complex formation has an effect both on the activation of the naive subset and on the polarization between Th17 and Tregs, demonstrating that the translational machinery controls many stages of T cell biology. We also show that acetyl-CoA conversion to malonyl-CoA, a central step in FAS, is controlled at the translational level rather than at the level of ACC1 phosphorylation. Our data, coupled with metabolomics, suggest that manipulation of T cell biology can be obtained through selective interventions on translation factors and ACC1.

Based on our work, translational control assumes a strong significance in T cells. Considering the fact that mTOR activation is a well-known controller of T cell biology (Delgoffe et al., 2009), and the well-known role of mTORC1 in the control of initiation of translation (Sonenberg and Hinnebusch, 2009), elongation (Faller et al., 2015), and metabolism (Ben-Sahra and Manning, 2017; Yang et al., 2013), we unveil a strong layer of translational control that explains how the rapid activation of a metabolic pathway can be achieved through the translation of pre-existing mRNAs. We have also found that in naive T cells, mRNAs encoding for metabolic enzymes were not adequately represented at the protein level. Similarly, we have shown for the first time that ACC1 mRNA levels were virtually identical in all subsets of freshly isolated *ex vivo* human $CD4^+$ T cells, but at the protein level, ACC1 was virtually undetectable in naive and easily detectable in the Th1 subset. All these data point to a lack of correspondence between mRNA and protein levels. It is unlikely that the mechanism of translational regulation that we report for metabolic enzymes is specific for this class of proteins. During differentiation of mouse $CD8^+$ T cells, translational inhibition of RP mRNAs occurs when cells stop dividing (Araki et al., 2017). In this respect the need for developing efficient analyses of the translatome, perhaps at the single-cell level, becomes essential.

The fact that during T cell activation, despite the large ATP variations observed, AMP/ATP ratios never change, puts further emphasis on the relevance of translational repression in the control of metabolism. ATP levels may remain high in view of the activation of oxidative phosphorylation (OXPHOS), in parallel with glycolysis. In many cell types, ACC1 is repressed by AMPK activation driven by high AMP/ATP ratios (Fullerton et al., 2013). However, such a mechanism would greatly impair the metabolic flexibility of T cells given that AMPK represses mTORC1 activation, which in turn affects many facets of T cell biology (Powell and Delgoffe, 2010). Hence, translational repression of ACC1 allows a shut-off of FAS without impairing the rapidity of mTORC1 activation in quiescent T cells. At later phases of T cell commitment, when the phenotype between effector and memory can be regulated by the intensity of mTORC1 signaling, the modulatory role of AMPK should emerge, as was actually shown in mice (Blagih et al., 2015).

One observation of our work is a clear difference between B cells and T cells in the context of eIF4E/4EBPs ratios. B cells contain more eIF4E than 4E-BPs, whereas T cells have more 4E-BPs than eIF4E. Since sensitivity to mTORC1 inhibition with rapamycin depends on the ratio between 4E-BPs and eIF4E (Alain et al., 2012; Grosso et al., 2011), this finding predicts the differential effects of rapamycin administration on the two cell types. However, not all translation passes through mTORC1 activation. eIF6, for instance, is rate limiting for translation and tumor growth independently of mTOR activation (Brina et al., 2015; Gandin et al., 2008; Miluzio et al., 2011). eIF6 requires activation by signaling pathways that converge on protein kinase C (Ceci et al., 2003). A rapid increase of eIF6 activity is observed upon T cell stimulation and contributes to the glycolytic switch (Manfrini et al., 2017), further demonstrating that overall T cell metabolism can be under translational control of other initiation factors. In addition, specific cytokine translation can be controlled by non-canonical RNA binding proteins, such as GAPDH with IFN-γ (Chang et al., 2013).

In the context of metabolism, our work suggests that metabolic fluxes of T cell subsets can be rather peculiar and reflect the inherent complexity of gene expression of these cells (Procaccini et al., 2016). Most of our observations are in line with a general model whereby T cell activation leads to an increase of both glycolysis and OXPHOS (Buck et al., 2016; Chang et al., 2013) starting from a G_0 level in which nutrients are very low. It is rather intriguing that some amino acids such as aspartate and glutamine are remarkably high in quiescent naive cells, whereas others such as asparagine are low. These data suggest that glutamine may also act as a primary energy source of quiescent cells, and aspartate is accumulated as a metabolite ready for nucleotide synthesis (Vazquez et al., 2016). Further studies are required. Upon activation, in line with other studies, we provide evidence on the importance of the FAS program for T cell polarization (Berod et al., 2014) and we further suggest that the FAS pathway sustains a feed-forward loop for glycolysis. In agreement with recent observations (Mak et al., 2017), we found increased oxidized glutathione (Table S6) predicting that glutathione is essential for late activation of T cells.

Finally, our data point to the risk of transcriptomics studies, which may fail to catch the real biology of T cell subsets if not associated with knowledge of pathway activation or protein studies. The ACC1 case is particularly exemplifying, as we find equal mRNA levels but totally different protein levels in effector and naive T cells.

In conclusion, we would like to speculate that naive T cells partly resemble oocytes ready to be activated which, upon fertilization, start a translational program impinging on a pre-accumulated ribosomal machinery and mRNAs. In this context, it will be interesting to find how mRNAs are stored, in view of emerging evidence that some metabolic enzymes can also act as mRNA binding proteins (Castello et al., 2015).

Limitations of Study

The use of human lymphocytes makes it difficult to dissect whether other metabolic factors, whose mRNAs in naive T cells were not adequately represented at the protein level, are indeed shut off at the translational level. The specific contribution of these factors on the metabolic profile remains to be determined. Further limitations to our data are the lack of information on the mechanism regulating translation of GLUT1 and the fact that metabolomics are limited to steady-state levels and would be strengthened by quantifying metabolite fluxes. Finally, to complete our data we should investigate whether the inhibition of the eIF4F complex in Th17 versus Treg cell development is not limited to ACC1 translation shutdown. We hope that future work will provide a deeper understanding of how translation controls the metabolism that dictates T cell fate.

STAR★METHODS

Detailed methods are provided in the online version of this paper and include the following:

- KEY RESOURCES TABLE
- CONTACT FOR REAGENT AND RESOURCE SHARING
- EXPERIMENTAL MODEL AND SUBJECT DETAILS
  - Human Primary T Cells

SUPPLEMENTAL INFORMATION

Supplemental Information includes six figures and six tables and can be found with this article online at https://doi.org/10.1016/j.cmet.2018.08.009.

ACKNOWLEDGMENTS

We thank S. Oliveto and A. Miluzio for discussions and suggestions. We thank the Blood Bank of Fondazione Istituto di Ricovero e Cura a Carattere Scientifico Ca' Granda Ospedale Maggiore Policlinico for providing us with human blood samples. This work was supported by grant ERC TRANSLATE 338999 and IG 2014 AIRC to S.B.

AUTHOR CONTRIBUTIONS

S.B., S.R., and N.M. designed the study. S.R. and N.M. conducted experiments and analyzed the data. S.B. and R.A. analyzed the data. R.A. and S.R. mined data and performed statistical analysis. S.B. helped in data analysis. M.C.C. performed FACS analysis of GLUT1. P.C. performed lactate, pyruvate, and OCR analysis. G.S. performed experiments on puromycin incorporation. M.P., S.A., and R.M. discussed the results and commented on the manuscript. S.R. and S.B. wrote the paper.

DECLARATION OF INTERESTS

The authors declare no competing interests.

Received: October 13, 2017
Revised: March 24, 2018
Accepted: August 7, 2018
Published: September 6, 2018; corrected online: September 20, 2018

REFERENCES

Alain, T., Morita, M., Fonseca, B.D., Yanagiya, A., Siddiqui, N., Bhat, M., Zammit, D., Marcus, V., Metrakos, P., Voyer, L.A., et al. (2012). eIF4E/4E-BP ratio predicts the efficacy of mTOR targeted therapies. Cancer Res. *72*, 6468–6476.

Araki, K., Morita, M., Bederman, A.G., Konieczny, B.T., Kissick, H.T., Sonenberg, N., and Ahmed, R. (2017). Translation is actively regulated during the differentiation of CD8+ effector T cells. Nat. Immunol. *18*, 1046–1057.

Ardawi, M.S., and Newsholme, E.A. (1984). Metabolism of ketone bodies, oleate and glucose in lymphocytes of the rat. Biochem. J. *221*, 255–260.

Ben-Sahra, I., and Manning, B.D. (2017). mTORC1 signaling and the metabolic control of cell growth. Curr. Opin. Cell Biol. *45*, 72–82.

Berod, L., Friedrich, C., Nandan, A., Freitag, J., Hagemann, S., Harmrolfs, K., Sandouk, A., Hesse, C., Castro, C.N., Bahre, H., et al. (2014). De novo fatty acid synthesis controls the fate between regulatory T and T helper 17 cells. Nat. Med. *20*, 1327–1333.

Biffo, S., Manfrini, N., and Ricciardi, S. (2018). Crosstalks between translation and metabolism in cancer. Curr. Opin. Genet. Dev. *48*, 75–81.

Biffo, S., Sanvito, F., Costa, S., Preve, L., Pignatelli, R., Spinardi, L., and Marchisio, P.C. (1997). Isolation of a novel beta4 integrin-binding protein (p27(BBP)) highly expressed in epithelial cells. J. Biol. Chem. *272*, 30314–30321.

Blagih, J., Coulombe, F., Vincent, E.E., Dupuy, F., Galicia-Vazquez, G., Yurchenko, E., Raissi, T.C., van der Windt, G.J., Viollet, B., Pearce, E.L., et al. (2015). The energy sensor AMPK regulates T cell metabolic adaptation and effector responses in vivo. Immunity *42*, 41–54.

Bonnal, R.J., Ranzani, V., Arrigoni, A., Curti, S., Panzeri, I., Gruarin, P., Abrignani, S., Rossetti, G., and Pagani, M. (2015). De novo transcriptome profiling of highly purified human lymphocytes primary cells. Sci. Data *2*, 150051.

Brina, D., Miluzio, A., Ricciardi, S., Clarke, K., Davidsen, P.K., Viero, G., Tebaldi, T., Offenhauser, N., Rozman, J., Rathkolb, B., et al. (2015). eIF6 coordinates insulin sensitivity and lipid metabolism by coupling translation to transcription. Nat. Commun. *6*, 8261.

Buck, M.D., O'Sullivan, D., Klein Geltink, R.I., Curtis, J.D., Chang, C.H., Sanin, D.E., Qiu, J., Kretz, O., Braas, D., van der Windt, G.J., et al. (2016). Mitochondrial dynamics controls T cell fate through metabolic programming. Cell *166*, 63–76.

Budde, K., Becker, T., Arns, W., Sommerer, C., Reinke, P., Eisenberger, U., Kramer, S., Fischer, W., Gschaidmeier, H., Pietruck, F., et al. (2011). Everolimus-based, calcineurin-inhibitor-free regimen in recipients of de-novo kidney transplants: an open-label, randomised, controlled trial. Lancet *377*, 837–847.

Cardaci, S., Zheng, L., MacKay, G., van den Broek, N.J., MacKenzie, E.D., Nixon, C., Stevenson, D., Tumanov, S., Bulusu, V., Kamphorst, J.J., et al. (2015). Pyruvate carboxylation enables growth of SDH-deficient cells by supporting aspartate biosynthesis. Nat. Cell Biol. *17*, 1317–1326.

Castello, A., Hentze, M.W., and Preiss, T. (2015). Metabolic enzymes enjoying new partnerships as RNA-binding proteins. Trends Endocrinol. Metab. *26*, 746–757.

Ceci, M., Gaviraghi, C., Gorrini, C., Sala, L.A., Offenhauser, N., Marchisio, P.C., and Biffo, S. (2003). Release of eIF6 (p27BBP) from the 60S subunit allows 80S ribosome assembly. Nature *426*, 579–584.

Chang, C.H., Curtis, J.D., Maggi, L.B., Jr., Faubert, B., Villarino, A.V., O'Sullivan, D., Huang, S.C., van der Windt, G.J., Blagih, J., Qiu, J., et al. (2013). Posttranscriptional control of T cell effector function by aerobic glycolysis. Cell *153*, 1239–1251.

Chantranupong, L., Scaria, S.M., Saxton, R.A., Gygi, M.P., Shen, K., Wyant, G.A., Wang, T., Harper, J.W., Gygi, S.P., and Sabatini, D.M. (2016). The CASTOR proteins are arginine sensors for the mTORC1 pathway. Cell *165*, 153–164.

Chi, H. (2012). Regulation and function of mTOR signalling in T cell fate decisions. Nat. Rev. Immunol. *12*, 325–338.

Delgoffe, G.M., Kole, T.P., Zheng, Y., Zarek, P.E., Matthews, K.L., Xiao, B., Worley, P.F., Kozma, S.C., and Powell, J.D. (2009). The mTOR kinase differentially regulates effector and regulatory T cell lineage commitment. Immunity *30*, 832–844.

Dibble, C.C., and Manning, B.D. (2013). Signal integration by mTORC1 coordinates nutrient input with biosynthetic output. Nat. Cell Biol. *15*, 555–564.

Dowling, R.J., Topisirovic, I., Alain, T., Bidinosti, M., Fonseca, B.D., Petroulakis, E., Wang, X., Larsson, O., Selvaraj, A., Liu, Y., et al. (2010).

mTORC1-mediated cell proliferation, but not cell growth, controlled by the 4E-BPs. Science *328*, 1172–1176.

Faller, W.J., Jackson, T.J., Knight, J.R., Ridgway, R.A., Jamieson, T., Karim, S.A., Jones, C., Radulescu, S., Huels, D.J., Myant, K.B., et al. (2015). mTORC1-mediated translational elongation limits intestinal tumour initiation and growth. Nature *517*, 497–500.

Fullerton, M.D., Galic, S., Marcinko, K., Sikkema, S., Pulinilkunnil, T., Chen, Z.P., O'Neill, H.M., Ford, R.J., Palanivel, R., O'Brien, M., et al. (2013). Single phosphorylation sites in Acc1 and Acc2 regulate lipid homeostasis and the insulin-sensitizing effects of metformin. Nat. Med. *19*, 1649–1654.

Gandin, V., Miluzio, A., Barbieri, A.M., Beugnet, A., Kiyokawa, H., Marchisio, P.C., and Biffo, S. (2008). Eukaryotic initiation factor 6 is rate-limiting in translation, growth and transformation. Nature *455*, 684–688.

Geginat, J., Sallusto, F., and Lanzavecchia, A. (2001). Cytokine-driven proliferation and differentiation of human naive, central memory, and effector memory CD4(+) T cells. J. Exp. Med. *194*, 1711–1719.

Geiger, R., Rieckmann, J.C., Wolf, T., Basso, C., Feng, Y., Fuhrer, T., Kogadeeva, M., Picotti, P., Meissner, F., Mann, M., et al. (2016). L-arginine modulates T cell metabolism and enhances survival and anti-tumor activity. Cell *167*, 829–842.e13.

Grosso, S., Pesce, E., Brina, D., Beugnet, A., Loreni, F., and Biffo, S. (2011). Sensitivity of global translation to mTOR inhibition in REN cells depends on the equilibrium between eIF4E and 4E-BP1. PLoS One *6*, e29136.

Henras, A.K., Soudet, J., Gerus, M., Lebaron, S., Caizergues-Ferrer, M., Mougin, A., and Henry, Y. (2008). The post-transcriptional steps of eukaryotic ribosome biogenesis. Cell Mol. Life Sci. *65*, 2334–2359.

Howell, J.J., Hellberg, K., Turner, M., Talbott, G., Kolar, M.J., Ross, D.S., Hoxhaj, G., Saghatelian, A., Shaw, R.J., and Manning, B.D. (2017). Metformin inhibits hepatic mTORC1 signaling via dose-dependent mechanisms involving AMPK and the TSC complex. Cell Metab. *25*, 463–471.

Hsieh, A.C., Liu, Y., Edlind, M.P., Ingolia, N.T., Janes, M.R., Sher, A., Shi, E.Y., Stumpf, C.R., Christensen, C., Bonham, M.J., et al. (2012). The translational landscape of mTOR signalling steers cancer initiation and metastasis. Nature *485*, 55–61.

Jump, D.B., Torres-Gonzalez, M., and Olson, L.K. (2011). Soraphen A, an inhibitor of acetyl CoA carboxylase activity, interferes with fatty acid elongation. Biochem. Pharmacol. *81*, 649–660.

Macintyre, A.N., Gerriets, V.A., Nichols, A.G., Michalek, R.D., Rudolph, M.C., Deoliveira, D., Anderson, S.M., Abel, E.D., Chen, B.J., Hale, L.P., et al. (2014). The glucose transporter Glut1 is selectively essential for CD4 T cell activation and effector function. Cell Metab. *20*, 61–72.

Mak, T.W., Grusdat, M., Duncan, G.S., Dostert, C., Nonnenmacher, Y., Cox, M., Binsfeld, C., Hao, Z., Brustle, A., Itsumi, M., et al. (2017). Glutathione primes T cell metabolism for inflammation. Immunity *46*, 675–689.

Manfrini, N., Ricciardi, S., Miluzio, A., Fedeli, M., Scagliola, A., Gallo, S., Brina, D., Adler, T., Busch, D.H., Gailus-Durner, V., et al. (2017). High levels of eukaryotic Initiation Factor 6 (eIF6) are required for immune system homeostasis and for steering the glycolytic flux of TCR-stimulated $CD4^+$ T cells in both mice and humans. Dev. Comp. Immunol. *77*, 69–76.

Masvidal, L., Hulea, L., Furic, L., Topisirovic, I., and Larsson, O. (2017). mTOR-sensitive translation: cleared fog reveals more trees. RNA Biol. *14*, 1299–1305.

Michie, C.A., McLean, A., Alcock, C., and Beverley, P.C. (1992). Lifespan of human lymphocyte subsets defined by CD45 isoforms. Nature *360*, 264–265.

Miluzio, A., Beugnet, A., Grosso, S., Brina, D., Mancino, M., Campaner, S., Amati, B., de Marco, A., and Biffo, S. (2011). Impairment of cytoplasmic eIF6 activity restricts lymphomagenesis and tumor progression without affecting normal growth. Cancer Cell *19*, 765–775.

Mitchell, C.J., Getnet, D., Kim, M.S., Manda, S.S., Kumar, P., Huang, T.C., Pinto, S.M., Nirujogi, R.S., Iwasaki, M., Shaw, P.G., et al. (2015). A multi-omic analysis of human naive $CD4^+$ T cells. BMC Syst. Biol. *9*, 75.

Moerke, N.J., Aktas, H., Chen, H., Cantel, S., Reibarkh, M.Y., Fahmy, A., Gross, J.D., Degterev, A., Yuan, J., Chorev, M., et al. (2007). Small-molecule inhibition of the interaction between the translation initiation factors eIF4E and eIF4G. Cell *128*, 257–267.

O'Neill, L.A., Kishton, R.J., and Rathmell, J. (2016). A guide to immunometabolism for immunologists. Nat. Rev. Immunol. *16*, 553–565.

Piccirillo, C.A., Bjur, E., Topisirovic, I., Sonenberg, N., and Larsson, O. (2014). Translational control of immune responses: from transcripts to translatomes. Nat. Immunol. *15*, 503–511.

Powell, J.D., and Delgoffe, G.M. (2010). The mammalian target of rapamycin: linking T cell differentiation, function, and metabolism. Immunity *33*, 301–311.

Procaccini, C., Carbone, F., Di Silvestre, D., Brambilla, F., De Rosa, V., Galgani, M., Faicchia, D., Marone, G., Tramontano, D., Corona, M., et al. (2016). The proteomic landscape of human ex vivo regulatory and conventional T cells reveals specific metabolic requirements. Immunity *44*, 406–421.

Reuter, J.S., and Mathews, D.H. (2010). RNAstructure: software for RNA secondary structure prediction and analysis. BMC Bioinformatics *15*, 129.

Rohrig, F., and Schulze, A. (2016). The multifaceted roles of fatty acid synthesis in cancer. Nat. Rev. Cancer *16*, 732–749.

Rudra, D., and Warner, J.R. (2004). What better measure than ribosome synthesis? Genes Dev. *18*, 2431–2436.

Saxton, R.A., and Sabatini, D.M. (2017). mTOR signaling in growth, metabolism, and disease. Cell *168*, 960–976.

Sonenberg, N., and Hinnebusch, A.G. (2009). Regulation of translation initiation in eukaryotes: mechanisms and biological targets. Cell *136*, 731–745.

Thoreen, C.C., Chantranupong, L., Keys, H.R., Wang, T., Gray, N.S., and Sabatini, D.M. (2012). A unifying model for mTORC1-mediated regulation of mRNA translation. Nature *485*, 109–113.

Trapnell, C., Williams, B.A., Pertea, G., Martazavi, A., Kwan, G., van Baren, M.J., Salzberg, S.L., Wold, B.J., and Pachter, L. (2010). Transcript assembly and quantification by RNA-Seq reveals unannotated transcripts and isoform switching during cell differentiation. Nat. Biotechnol. *28*, 511–515.

Vazquez, A., Kamphorst, J.J., Markert, E.K., Schug, Z.T., Tardito, S., and Gottlieb, E. (2016). Cancer metabolism at a glance. J. Cell Sci. *129*, 3367–3373.

Wang, L., Wang, X., and Proud, C.G. (2000). Activation of mRNA translation in rat cardiac myocytes by insulin involves multiple rapamycin-sensitive steps. Am. J. Physiol. Heart Circ. Physiol. *278*, H1056–H1068.

Wang, R., Dillon, C.P., Shi, L.Z., Milasta, S., Carter, R., Finkelstein, D., McCormick, L.L., Fitzgerald, P., Chi, H., Munger, J., et al. (2011). The transcription factor Myc controls metabolic reprogramming upon T lymphocyte activation. Immunity *35*, 871–882.

Wang, R., and Green, D.R. (2012). Metabolic checkpoints in activated T cells. Nat. Immunol. *13*, 907–915.

Wolfson, R.L., Chantranupong, L., Saxton, R.A., Shen, K., Scaria, S.M., Cantor, J.R., and Sabatini, D.M. (2016). Sestrin2 is a leucine sensor for the mTORC1 pathway. Science *351*, 43–48.

Xia, J., Sinelnikov, I., Han, B., and Wishart, D.S. (2015). MetaboAnalyst 3.0 - making metabolomics more meaningful. Nucleic Acids Res. *43*, W251–W257.

Yang, K., Shrestha, S., Zeng, H., Karmaus, P.W., Neale, G., Vogel, P., Guertin, D.A., Lamb, R.F., and Chi, H. (2013). T cell exit from quiescence and differentiation into Th2 cells depend on Raptor-mTORC1-mediated metabolic reprogramming. Immunity *39*, 1043–1056.

STAR★METHODS

KEY RESOURCES TABLE

REAGENT or RESOURCE	SOURCE	IDENTIFIER
Antibodies		
Human CD4 (VIT-4)-VioGreen	Miltenyi	RRID: AB_2660918
Human CD45RO-APC (clone UCHL1)	Exbio	RRID: AB_10732749
Human CD62L-Pe-Cy5	BD Biosciences	RRID: AB_395929
Human CD3	BD Biosciences	RRID: AB_395742
Human CD28	BD Biosciences	RRID: AB_396068
Human Il-17A-PE	eBiosciences	RRID: AB_1724136
Human Il-17A- Pacific Blue	BioLegend	RRID: AB_961392
Human Foxp3-APC (clone PCH101)	eBiosciences	RRID: AB_1603281
Human Foxp3-Pacific Blue	BioLegend	RRID: AB_2104902
Human RORγt-APC	Invitrogen	RRID: AB_10609207
Human IL-4	R&D Systems	RRID: AB_2126744
Human IL-12	R&D Systems	RRID: AB_2123616
Human Glut1-FITC	R&D Systems	RRID: AB_2191041
Human Phospho-S6 Ribosomal Protein (ser235/236)	Cell Signaling	RRID: AB_331679
Human RACK1	BD Biosciences	RRID: AB_395577
Human Acetyl-CoA Carboxylase	Cell Signaling	RRID: AB_10694239
Human Phospho Acetyl-CoA Carboxylase (ser79)	Cell Signaling	RRID: AB_330337
Human AMPK	Cell Signaling	RRID: AB_330331
Human Phospho-AMPK (thr172)	Cell Signaling	RRID: AB_331250
Human TIM	Santa Cruz	RRID: AB_2256422
Human Vinculin	Millipore	RRID: AB_309711
Human Actin	Sigma	RRID: AB_476697
Human Puromycin Alexa Fluor 488 Conjugate (clone 12D10)	Millipore	RRID: AB_2736875
Chemicals, Peptides, and Recombinant Proteins		
Recombinant human interleukin-2	Miltenyi	Cat#130-097-748
Recombinant human interleukin-6	Miltenyi	Cat#130-095-365
Recombinant human interleukin-23	Miltenyi	Cat#130-095-757
Recombinant human interleukin-1b	Miltenyi	Cat#130-095-374
Human TGF-β1	Miltenyi	Cat#130-108-971
Phorbol 12-myristate 13-acetate (PMA)	Sigma	Cat#P1585
Ionomycin	Sigma	Cat#I0634
Sucrose	VWR Chemicals	Cat#57-50-1
Puromycin	Sigma	Cat#P7255
Soraphen A	Rolf Müller	Berod et al., 2014
Cycloheximide	Sigma	Cat#C7698
Actinomycin D	Sigma	Cat#A9415
Rapamycin	Sigma	Cat#R8781
4EGi-1	Tocris Bioscience	Cat#4800
Critical Commercial Assays		
$CD4^+$ T cell isolation kit	Miltenyi	Cat#130-096-533
CellTrace CFSE Cell Proliferation Kit	Invitrogen	Cat#C34554
Lactate Colorimetric/Fluorometric assay kit	Biovision	Cat#K607-100
Pyruvate assay kit	Biovision	Cat#K609-100
Extracellular Oxygen Consumption assay kit	Abcam	Cat#AB197243

(*Continued on next page*)

Continued		
REAGENT or RESOURCE	SOURCE	IDENTIFIER
Dual-Luciferase Reporter Assay System	Promega	Cat#E1910
Deposited Data		
E-MTAB-2319	(Bonnal et al., 2015)	https://www.ebi.ac.uk/arrayexpress/experiments/E-MTAB-2319/
Experimental Models: Cell Lines		
Human: primary T lymphocytes	This paper	N/A
Oligonucleotides		
Human GLUT1 (TaqMan)	Applied Biosystem	CAT#Hs00892681_m1
Human ACC1 (TaqMan)	Applied Biosystem	CAT#Hs01046047_m1
Eukaryotic 18S rRNA (TaqMan)	Applied Biosystem	CAT#4333760F
Human FOXP3 (Taqman)	Applied Biosystem	CAT#Hs01085834_m1
Human RORc (Taqman)	Applied Biosystem	CAT#Hs01076112_m1
Human Actin (Sybrgreen)	Metabion	F 5'- AGAGCTACGAGCTGCCTGAC-3', R 5'-CGTGGATGCCACAGGACT-3'
Human RPS29 (Sybrgreen)	Metabion	F 5'- TCTCGCTCTTGTCGTGTCTG-3', R 5'- CCGATATCCTTCGCGTACTG -3'
Human Renilla (Sybrgreen)	Metabion	F 5'- GGAATTATAATGCTTATCTACGTGC-3', R 5'- CTTGCGAAAAATGAAGACCTTTTAC-3'
Software and Algorithms		
R environment for statistical computing	N/A	https://www.r-project.org/
Cufflinks	Trapnell et al. (2010)	http://cole-trapnell-lab.github.io/cufflinks/
Microsoft Excel	Microsoft	https://www.microsoft.com/
MetaboAnalyst 3.0	Xia et al. (2015)	http://www.metaboanalyst.ca/
RNAStructure	Reuter and Mathews (2010)	https://rna.urmc.rochester.edu/RNAstructureWeb/Servers/Predict1/Predict1.html

CONTACT FOR REAGENT AND RESOURCE SHARING

Further information and requests for reagents may be directed to and will be fulfilled by the Lead Contact, Stefano Biffo (biffo@ingm.org).

EXPERIMENTAL MODEL AND SUBJECT DETAILS

Human Primary T Cells

Blood was provided by Fondazione Istituto di Ricovero e Cura a Carattere Scientifico Ca'Granda Ospedale Maggiore Policlinico in Milan. The blood was taken from healthy donors, regardless of sex, because gender identity of the donors is not relevant for the results of the experiments. The age of healthy donors was unknown for privacy reasons. All experiments performed on human blood samples were approved by the ethics committee of Fondazione Istituto di Ricovero e Cura a Carattere Scientifico Ca'Granda Ospedale Maggiore Policlinico and informed consent was obtained from all subjects.

METHOD DETAILS

Isolation of Human Primary Lymphocyte Subsets

Human primary lymphocyte subsets were isolated *ex vivo* from human blood samples by ficoll-hypaque density-gradient centrifugation followed by FACS sorting for a various combination of surface markers (Bonnal et al., 2015). The purity of the isolated cells was >95%.

Human $CD4^+$ T Cell Culture

After ficoll-hypaque density-gradient centrifugation, $CD4^+$ T cells were enriched by magnetic separation (AutoMACS, Miltenyi Biotec) using human $CD4^+$ T Cell Isolation Kit (Miltenyi Biotec) and further purified by FACS sorting for live $CD4^+CD62L^+CD45RO^-$ naïve

T cells. Naïve $CD4^+$ T cells were then activated with Dynabeads Human T-Activator anti-CD3/anti-CD28 beads (1 bead/cell, Life Technologies) and cultured for the indicated time intervals in RPMI 1640 medium (Life Technologies) at 37°C in 5% CO_2 environment. Interleukin 2 (IL-2) was added at 20 IU/ml (202-IL; R&D Systems).

For cytokine secretion analysis, cells were treated with 10 μM 4EGi-1 for 24 h after 48 h of Dynabeads stimulation.

In Vitro Th17-Cell Differentiation

In vitro differentiation of Th17 cells was performed at 5000 cells/well in 96 well plate-bound anti-CD3 (0.02 mg/mL, BD Biosciences) and anti-CD28 antibodies (6 mg/mL, BD Biosciences) in Dulbecco modified Eagle medium (5% human serum, 1 mmol/L sodium pyruvate, 10 mmol/L nonessential amino acids, 1% penicillin/streptomycin, and 25 mmol/L b-mercaptoethanol). Cells were cultured for 6 days under Th17-promoting conditions with neutralizing antibodies against IFN-γ, IL-12 and IL-4 and recombinant human TGF-β1, IL-1b, IL-6, and IL-23 at 37°C in 5% CO_2 environment. All neutralizing antibodies (R&D Systems) were added at 2 mg/mL. All recombinant cytokines (Miltenyi) were added at 10 ng/mL, with the exception of TGF-β1, which was used at 1 ng/mL.

Where indicated, cells were treated with 10 μM 4EGi-1 after 2 days under Th17-promoting conditions.

For shRNA experiments, cells were infected after 2 days under Th17-promoting conditions with scramble shRNA in pGIPZ lentivirus vector or eIF4E-shRNA in pGIPZ lentivirus vectors. Mature antisense sequence was: 5'-TAAATTACTAGACAACTGG-3' (Open Biosystem).

Polysomal Profiles

Polysomal profiles were performed as follow. Cells were lysed in 30 mM Tris-HCl, pH 7.5, 100 mM NaCl, 30 mM $MgCl_2$, 0.1% NP-40, 100 μg/ml cycloheximide and 30 U/ml RNasin. Lysates were clarified at 12,000 r.p.m. for 10 min at 4°C and cytoplasmic extracts with equal amounts of RNA were loaded on a 15-50% sucrose gradient and centrifuged at 4°C in a SW41Ti Beckman rotor for 3 h 30 min at 39,000 r.p.m. Absorbance at 254 nm was recorded by BioLogic LP software (BioRad) and fractions (1 ml each) were collected for subsequent RNA extraction.

Where indicated, cells were treated with 50 μM 4EGi-1 or 100 nM Rapamycin for 4 h after 68 h of Dynabeads stimulation.

RNA Extraction and Quantitative RT-PCR

Total RNA from cells was extracted with TRIzol reagent (Invitrogen). For total, subpolysomal and polysomal RNA extractions from sucrose gradient aliquotes, samples were incubated with 100μg/mL proteinase K and 1% SDS for 2 h at 37°C. RNA was then extracted by phenol/chloroform/isoamyilic acid method. After treatment of RNA with RQ1 RNase-free DNase (Promega), reverse transcription was performed according to SuperScript III First-Strand Synthesis kit (Invitrogen). Real-time PCR amplification and analysis was conducted in StepOnePlus Real-Time PCR System (Thermo Fisher Scientific) using pre-designed probe sets and Taqman Universal PCR Master Mix (Applied Biosystems).

Synthesis of Plasmids, Cell Transfection and Luciferase Assays

The RL ACC1 5'-UTR plasmid was obtained by cloning the 5'-UTR of ACC1 isoform 2 (ENST00000616317.4) at the Nhe1 site of the *Renilla* Luciferase reporter (pRL) plasmid. For transient transfection, cells were seeded into 6-well plates 24 h before transfection. HEK293 cells were transfected with either the PRL or the RL ACC1 5'-UTR plasmids using calcium phosphate. After 24 h transfection period, the medium was changed to fresh DMEM supplemented with 25 μM 4EGi-1 or 0,05% DMSO, as a control.

Renilla Luciferase activity was detected using the DualGlo Luciferase System (Promega) and values were normalized on renilla Firefly mRNA abundance.

SUnSET Assay

For protein synthesis measurements, $CD4^+$ naïve and $CD4^+$ T cells stimulated *in vitro* for 72 h were treated with 5 μg/ml puromycin for 10 min and fixed at 4°C with Fixation Buffer (eBioscience). Fixed cells were stained with FITC-conjugated anti-puromycin Ab (Millipore). Puromycin incorporation was measured by flow cytometry (FACSCanto II, BD Bioscience) and data were analysed with FlowJo software.

Immunofluorescence

For immunofluorescence based imaging, cells were fixed with 3% paraformaldehyde, permeabilized with 0.1% Triton X-100, blocked with PBST (PBS containing 1% bovine serum albumin and 0.1% Tween-20) and incubated with antibodies in PBST against the indicated proteins overnight at 4°C.

Primary antibodies were used at the following dilutions: rabbit polyclonal anti-phospho-rpS6 (ser235/236) (1:100; Cell Signaling), mouse anti-RACK1 (1:200, Becton Dickinson). Alexa Fluor 488- and Alexa Fluor 555-conjugated secondary antibodies (1:500, Thermo Fisher Scientific) were added for 1 h at room temperature. Slides were mounted in Mowiol 4-88 mounting medium (Sigma-Aldrich).

Fluorescence images were acquired using a confocal microscope (Leica TCS SP5) at 1,024 Å~ 1,024 dpi resolution. All the images were further processed with Photoshop CS6 (Adobe) software.

Assessment of GLUT1 Expression by Flow Cytometry

Analysis of GLUT1 expression was conducted both in cells isolated *ex vivo* and stimulated *in vitro* for the indicated time intervals. In both cases, cells were fixed at 4°C with Fixation Buffer (eBioscience). Fixed cells were stained with FITC-conjugated anti-GLUT1 Ab (R&D Systems). Mouse IgG2β was used as an isotype control. GLUT1 staining was measured by flow cytometry (FACSCanto II, BD Bioscience) and data were analysed with FlowJo software.

Where indicated, cells were treated with 100 μg/ml cycloheximide or 5 μg/ml actinomycin D for 4 h after 20 h of Dynabeads stimulation.

Western Blotting

Whole-cell lysates were prepared using RIPA buffer (10 mM Tris-HCl, pH 7.4, 1% sodium deoxycholate, 1% TritonX-100, 0.1% SDS, 150 mM NaCl and 1 mM EDTA, pH 8.0) supplemented with complete Protease Inhibitor Cocktail Roche Applied Science). Cell lysates were separated by SDS-PAGE and transferred to polyvinylidene fluoride membranes (Merck Millipore). Immunoblotting was performed using rabbit anti-phospho-rpS6 (ser235/236) (1:1,000; Cell Signaling), rabbit anti-Acetyl-CoA-Carboxylase (1:1,000, Cell Signaling, clone C83B10), rabbit anti-phospho-Acetyl-CoA-Carboxylase (ser79) (1:1,000, Cell Signaling), rabbit anti-AMPK (1:1,000, Cell Signaling), rabbit anti-phospho-AMPK (thr172) (1:1,000, Cell Signaling), mouse anti-TIM (1:1,000, Santa Cruz), mouse anti-Vinculin (1:1,000, Millipore), mouse anti-α-Actin (1:4,000, Sigma) and goat anti-rabbit and goat-mouse horseradish peroxidase (1:5,000, Santa Cruz) and detected using ECL prime (GE Healthcare).

For ACC1 protein expression analysis, cells were treated with Rapamycin (100 nM), added at the onset of the cultures, 100 μg/ml cycloheximide or 5 μg/ml actinomycin D for 24 h after 24 h of Dynabeads and with 10 μM 4EGi-1 for 48 h or 24 h after 24 h or 48 h of Dynabeads stimulation, respectively.

Mass Spectrometry-Based Targeted Metabolomics

The metabolomic profiling was performed by Metabolomics Analysis Service (Yamagata, JP). For metabolite extraction, 10^7 cells were harvested for each time points, centrifuged at 1,200 r.p.m. for 2 min and pellets washed in 5% mannitol. Pellets were resuspended in 800 μl of methanol and mixed by vortexing. Internal standard solution was added to the mix and samples were centrifuged at 2,300 g at 4°C for 5 min. Supernatants were purified by centrifugation on Centrifugal Filter Units. Metabolite extracts were analyzed by Carcinoscope CE-TOF/QcQ MS. Metabolite amounts are given as pmol per 10^6 cells.

Lactate Secretion Assay

Cells were maintained in high-glucose medium for 24 h and then switched to serum-free high-glucose (4,5 g/L) for 4h as indicated in Brina et al. (2015). Lactate secreted into the medium was measured using a fluorogenic kit (BioVision). Average of fluorescence intensity was calculated for each condition replicates. Values were normalized to cell number.

Where indicated, cells were treated with 200 nM Soraphen A, added at the onset of culture, or 10 μM 4EGi-1 for 24 h after 48 h of Dynabeads stimulation.

Extracellular O_2 Consumption Assay

The extracellular oxygen consumption was measured using a fluorogenic kit (Abcam) according to manufacturer protocols. Average of fluorescence intensity was calculated for each replicate, and then values were normalized for cells number.

Where indicated, cells were treated with 200 nM Soraphen A, added at the onset of colture, or 10 μM 4EGi-1 for 24 h after 48 h of Dynabeads stimulation.

Pyruvate Levels Assay

Intracellular pyruvate analysis was measure using fluorogenic kit (BioVision) according to manufacturer protocol. Average of fluorescence intensity was calculated for each replicate, and then values were normalized for protein content obtained.

Where indicated, cells were treated with 200 nM Soraphen A, added at the onset of culture, or 10 μM 4EGi-1 for 24 h after 48 h of Dynabeads stimulation.

QUANTIFICATION AND STATISTICAL ANALYSIS

RNA-Seq Analysis

All RNA-seq data were retrieved from Bonnal et al. (2015) (ArrayExpress: E-MTAB-2319 experiment). Gene expression levels were estimated by Cufflinks (version 2.0.2) as raw FPKM counts.

The analysis of metabolic genes expression levels between $CD4^+$ and $CD8^+$ cell subsets was conducted using the pair wise Pearson's correlation within the R environment. The matrix of Pearson's correlation coefficients for all possible pairs of subset was calculated using the rcorr function from the *Hmisc* R library. The Pearson's correlation matrix was represented through a heatmap, were the correlation coefficients were shown for each pair of subset.

Proteomic Analysis

All the proteomic data were retrieved from Mitchell et al. (2015). Protein expression values (iBAQ) were obtained through the iTRAQ based methodology, which provides an intensity-based absolute measure of protein abundance between samples. To compare mRNA and protein levels, we represented in a plot iBAQ intensities (proteome) versus FPKM values.

Metabolomic Analysis

Heatmap of metabolites concentration was generated within the R environment using the heatmap.2 function from the *gplots* library.

Principle Component Analysis (PCA) of metabolomics data was obtained using the MetaboAnalyst 3.0 tool suite. The metabolite concentration values were log transformed according to generalized logarithm transformation (glog) proposed by MetaboAnalyst. In the PCA plot the 95% confidence regions are shown.

Statistical Analysis

Analyses were performed with Excel (Microsoft) software. All data are shown as mean values ± SD. Statistically significant differences were determined using the Student's t test. $p<0.05$ was considered to indicate statistical significance. Correlations were evaluated using the Pearson r method. Statistical parameters, including the value of n, are noted in figure legends.

DATA AND SOFTWARE AVAILABILITY

The metabolomics data are available in Table S6.